Closed-Loop Control of Compensation Point in the K-Rb-^{21}Ne Comagnetometer

Liwei Jiang,[1] Wei Quan,[1,2,*] Feng Liu,[1] Wenfeng Fan,[1] Li Xing,[1] Lihong Duan,[1] Wuming Liu,[3,4,†] and Jiancheng Fang[1,2]

[1] *School of Instrumentation and Optoelectronic Engineering, Beihang University, Beijing 100191, China*
[2] *Science and Technology on Inertial Laboratory, Beihang University, Beijing 100191, China*
[3] *Beijing National Laboratory for Condensed Matter Physics, Institute of Physics, Chinese Academy of Sciences, Beijing 100190, China*
[4] *School of Physical Sciences, University of Chinese Academy of Sciences, Beijing 100190, China*

(Received 19 November 2018; revised manuscript received 26 June 2019; published 9 August 2019)

We investigate the real-time closed-loop control of the compensation point in a K-Rb-^{21}Ne comagnetometer operated in the spin-exchange relaxation-free regime. By locking the electron resonance, the alkali-metal electrons are free from the fluctuations of the longitudinal ambient magnetic field and nuclear magnetization, which could improve the systematic stability, enlarge the linear measuring range, and suppress the cross-talk error of the comagnetometer. The demonstration of closed-loop control of the magnetic field in the single nuclear species comagnetometer is of great significance for rotation sensing such as in gyroscopes and other high-precision metrology applications of the comagnetometer.

DOI: 10.1103/PhysRevApplied.12.024017

I. INTRODUCTION

Atomic comagnetometers, which use at least two spin species to measure magnetic fields in the same space and time, have been found to have a wide range of applications, such as tests of *CPT* and Lorentz invariance [1–4], searches for anomalous spin-dependent forces [5–8], and inertial rotation sensing [9–13]. In all of these applications, the long-term stability of the comagnetometer is essential and often limited by noise and systematic effects associated with the external magnetic fields and magnetization due to spin dipolar interactions [14,15]. In general, comagnetometers with two or more nuclear species calculate an appropriate combination of nuclear precession frequencies to cancel out magnetic field dependence [16–18]. Based on the dual nuclear isotopes differential technique, a three-axis residual magnetic field closed-loop control system has been incorporated in NMR gyros to guarantee the long-term stability of magnetic fields [19–21].

However, it is a challenging and unexplored topic to control magnetic field fluctuations in the single nuclear species comagnetometers. The primary difficulty is acquiring magnetic field information as the feedback signal without the exterior sensors. To circumvent spin precession due to magnetic fields as well as their gradients, the spin-exchange relaxation-free (SERF) comagnetometer involving alkali metals and one kind of nuclear species was first introduced in Ref. [22]. A bias magnetic field parallel to the pump laser beam, which is referred to as the compensation point, cancels the fields from electron and nuclear magnetization and operates the atomic spins in a self-compensating regime, where the nuclear magnetization adiabatically follows slow changes in the external magnetic field, decreasing the effect of transverse fields on alkali metal electron spins [9,23,24]. The compensation point also operates the high-density alkali-metal atoms in a low magnetic field, such that the spin-exchange rate is much larger than the Larmor precession frequency and the spin-exchange relaxation is suppressed [25,26]. This process allows a SERF magnetometer to detect the precession of noble gas atoms with high sensitivity. Despite the sensitivity to magnetic fields that has been suppressed by the self-compensating effect in the SERF comagnetometer, the drifts of external magnetic fields still exert a significant influence on the systematic stability [27]. Moreover, the fluctuation of the compensation point also causes a cross-talk error in the dual-axis SERF comagnetometer [28,29]. The applications of the SERF comagnetometer confront considerable obstacles due to the uncontrolled compensation of the magnetic field in the system.

Among the SERF comagnetometers, the K-Rb-^{21}Ne comagnetometer has the potential for higher sensitivity by virtue of the lower gyromagnetic ratio of ^{21}Ne compared to other noble gases, such as ^{3}He and ^{129}Xe [3,9]. Additionally, the K-Rb hybrid pumping technique is adopted to

*quanwei@buaa.edu.cn
†wliu@iphy.ac.cn

 © 2019 American Physical Society

achieve more homogeneous polarization of alkali metals and higher pumping efficiency of ^{21}Ne [30,31]. Therein, the optically thin K atoms are homogeneously polarized by the pump laser. The optically dense Rb atoms are polarized by spin-exchange collisions with the polarized K atoms; then they hyperpolarize the noble gas ^{21}Ne. Here, in order to improve the performance of the K-Rb-^{21}Ne comagnetometer, we demonstrate a real-time closed-loop control method to stabilize the compensation point. We find that the electron resonance is shifted to a high frequency and separated clearly from the nuclear resonance owing to the large field from electron magnetization in the K-Rb-^{21}Ne comagnetometer. The electron resonance frequency and phase scale with the shift of the compensation point, which allows us to achieve closed-loop control of the compensation point by locking the electron resonance. This method is validated theoretically and experimentally in our dual-axis K-Rb-^{21}Ne comagnetometer. With the closed-loop control of the compensation point, the alkali-metal electrons are immune to the fluctuations of the longitudinal ambient magnetic field and nuclear magnetization, which could improve the systematic stability, enlarge the linear measuring range, and suppress the cross-talk error of the comagnetometer.

II. THEORY

In the K-Rb-^{21}Ne comagnetometer, as the density of Rb atoms is much higher than that of K atoms and Rb atoms are probed, the behavior of the comagnetometer can be approximately described by a set of coupled Bloch equations for electron spin polarization $\mathbf{P^e}$ of Rb and nuclear spin polarization $\mathbf{P^n}$ of ^{21}Ne [9],

$$\frac{\partial \mathbf{P^e}}{\partial t} = \mathbf{\Omega} \times \mathbf{P^e} + \frac{\gamma_e}{Q}\left(\mathbf{B} + \lambda M_n \mathbf{P^n} + \mathbf{L}\right) \times \mathbf{P^e} + \frac{1}{Q}\left(R_{\rm pu}\mathbf{s_{pu}} + R_{\rm se}^{\rm en}\mathbf{P^n} + R_m \mathbf{s_{pr}} - R_{\rm tot}^{e}\mathbf{P^e}\right), \quad (1)$$

$$\frac{\partial \mathbf{P^n}}{\partial t} = \mathbf{\Omega} \times \mathbf{P^n} + \gamma_n\left(\mathbf{B} + \lambda M_e \mathbf{P^e}\right) \times \mathbf{P^n} + R_{\rm se}^{\rm ne}\left(\mathbf{P^e} - \mathbf{P^n}\right) - R_{\rm sd}^{n}\mathbf{P^n}. \quad (2)$$

The above Bloch equations are written in the rotating frame, where $\mathbf{\Omega}$ is the inertial rotation rate vector; $\gamma_e = 2\pi \times 28$ Hz/nT and $\gamma_n = 2\pi \times 0.00336$ Hz/nT are the gyromagnetic ratios of the electron spins and nuclear spins, respectively; Q is the nuclear slowing-down factor and is a function of the electron polarization [32]; $\mathbf{B}$ is the ambient magnetic field vector; $\lambda = 8\pi\kappa_0/3$ is the geometrical factor containing the enhancement factor κ_0, arising from the overlap of the alkali-metal electron wave function and the noble-gas nucleus [33]; M_e and M_n are the magnetization of electron spins and nuclear spins corresponding to full spin polarization, which are proportional to the atom number density; $\mathbf{L}$ is the light shift (ac-Stark shift) field arising from the pump and probe lasers; $R_{\rm se}^{\rm en}$ and $R_{\rm se}^{\rm ne}$ are the spin-exchange rates of the nucleus and the electron with each other; $R_{\rm pu}$ and R_m are the pumping rates of the pump and probe laser beams; $\mathbf{s_{pu}}$ and $\mathbf{s_{pr}}$ are the optical pumping vectors, which give the directions and magnitudes of photon spin polarizations; $R_{\rm tot}^{e}$ is the total relaxation rate for electrons, defined as $R_{\rm tot}^{e} = R_{\rm pu} + R_m + R_{\rm se}^{\rm en} + R_{\rm sd}^{e}$, where $R_{\rm sd}^{e}$ is the electron spin-destruction rate; and $R_{\rm sd}^{n}$ is the nuclear spin-destruction rate.

Here, we adopt a series of approximations to make the solution of Eqs. (1) and (2) more tractable, retaining the main features that determine the high-accuracy behavior of the coupled dynamics. The electron spins and nuclear spins are polarized along the z axis. For small transverse excitations of the spins, the angles of polarization vectors $\mathbf{P^e}$ and $\mathbf{P^n}$ with respect to the z axis are small enough, so that we approximately assume the longitudinal polarization components P_z^e and P_z^n as constants [34]. Ignoring the transverse pumping rate of the pump laser, the pumping rate of the probe laser, and the transverse alkali-metal noble-gas spin-exchange terms, the Bloch equation for the transverse electron polarization $\tilde{P}^e = P_x^e + iP_y^e$, according to Eq. (1), can be simplified to

$$\frac{\partial \tilde{P}^e}{\partial t} = (i\omega_z - \Gamma)\,\tilde{P}^e - i\tilde{\omega}P_z^e, \quad (3)$$

where $\tilde{\omega} = \omega_x + i\omega_y$, $\omega_\alpha = \gamma_e\left(B_\alpha + \lambda M_n P_\alpha^n + L_\alpha\right)/Q + \Omega_\alpha$ $(\alpha = x, y, z)$, and $\Gamma = R_{\rm tot}^{e}/Q$.

We investigate the transverse oscillating magnetic field response of the K-Rb-^{21}Ne comagnetometer, especially focusing on the electron resonance. So an oscillating field $\tilde{\omega}_1 \cos(\omega t)$, where $\tilde{\omega}_1 = \gamma_e\left(B_{x1} + iB_{y1}\right)/Q$, is applied in the transverse plane, whose frequency is much higher than the nuclear resonance frequency. Since the relaxation rate of the noble gas is small, the nuclear spins do not respond to this high-frequency modulation and just couple with the electron spins at a low frequency or steady state [12]. Equation (3) can be solved in a straightforward manner for oscillatory solutions in the complex form. Considering both a corotating $e^{i\omega t}$ and counter-rotating $e^{-i\omega t}$ response, the transverse electron polarization $\tilde{P}^e$ can be expressed by

$$\tilde{P}^e = \frac{i\tilde{\omega}_0 P_z^e}{i\omega_z - \Gamma} + \frac{i\tilde{\omega}_1 P_z^e e^{i\omega t}}{2\,(i\omega_z - i\omega - \Gamma)} + \frac{i\tilde{\omega}_1 P_z^e e^{-i\omega t}}{2\,(i\omega_z + i\omega - \Gamma)}, \quad (4)$$

where the first term describes the response to the dc (zero frequency) field and $\tilde{\omega}_0 = \omega_{x0} + i\omega_{y0}$.

The noble-gas nuclear spins are approximately operated at the steady state and Eq. (2) can be solved by setting the left-hand side to 0. The noble-gas nuclear spins couple with alkali-metal electron spins by spin-exchange interactions, which generate an effective magnetic field for

electron spins to precess under. When inputting rotation rate Ω_y, the nuclear spins produce an effective magnetic field $B_y^n = -\Omega_y/\gamma_n$. When inputting rotation rate Ω_x, the nuclear spins produce an effective magnetic field $B_x^n = -\Omega_x/\gamma_n$ [12]. As the oscillating field is applied along the y axis, we set $B_{x1} = 0$ and $B_{y1} = B_0$. With the ambient magnetic field compensated by coils and the light shift field eliminated [29], the polarization components $P_x^e = \mathrm{Re}[\tilde{P}^e]$ measured by the probe beam along the x axis and $P_y^e = \mathrm{Im}[\tilde{P}^e]$ measured by the probe beam along the y axis are given by

$$P_x^e = \frac{-\gamma_e P_z^e R_{\mathrm{tot}}^e}{D_s}\left(\frac{\Omega_y}{\gamma_n}+\frac{\gamma_e \delta B_z \Omega_x}{\gamma_n R_{\mathrm{tot}}^e}\right) + \frac{\gamma_e B_0 P_z^e}{2}\left[\frac{R_{\mathrm{tot}}^e \cos(\omega t) + \left(Q\omega - \gamma_e B_e^{\mathrm{eff}}\right)\sin(\omega t)}{\left(Q\omega - \gamma_e B_e^{\mathrm{eff}}\right)^2 + {R_{\mathrm{tot}}^e}^2} + \frac{R_{\mathrm{tot}}^e \cos(-\omega t) - \left(Q\omega + \gamma_e B_e^{\mathrm{eff}}\right)\sin(-\omega t)}{\left(Q\omega + \gamma_e B_e^{\mathrm{eff}}\right)^2 + {R_{\mathrm{tot}}^e}^2}\right], \quad (5)$$

$$P_y^e = \frac{\gamma_e P_z^e R_{\mathrm{tot}}^e}{D_s}\left(\frac{\Omega_x}{\gamma_n} - \frac{\gamma_e \delta B_z \Omega_y}{\gamma_n R_{\mathrm{tot}}^e}\right) + \frac{\gamma_e B_0 P_z^e}{2}\left[\frac{-\left(Q\omega - \gamma_e B_e^{\mathrm{eff}}\right)\cos(\omega t) + R_{\mathrm{tot}}^e \sin(\omega t)}{\left(Q\omega - \gamma_e B_e^{\mathrm{eff}}\right)^2 + {R_{\mathrm{tot}}^e}^2} + \frac{\left(Q\omega + \gamma_e B_e^{\mathrm{eff}}\right)\cos(-\omega t) + R_{\mathrm{tot}}^e \sin(-\omega t)}{\left(Q\omega + \gamma_e B_e^{\mathrm{eff}}\right)^2 + {R_{\mathrm{tot}}^e}^2}\right], \quad (6)$$

where $D_s = {R_{\mathrm{tot}}^e}^2 + \gamma_e^2\left[\delta B_z{}^2 + (\Omega_x/\gamma_n)^2 + \left(\Omega_y/\gamma_n\right)^2\right]$. Under the normal comagnetometer operation, a bias magnetic field $B_c = -B_n - B_e$ called the compensation point is applied parallel to the direction of the pump beam to cancel the field from nuclear magnetization $B_n = \lambda M_n P_z^n$ and the field from electron magnetization $B_e = \lambda M_e P_z^e$. Note that B_n and B_e are negative owing to the negative magnetization M_n and M_e. δB_z is the residual magnetic field with respect to the compensation point along the z axis. When the residual magnetic field inside the shields and light shift field is completely compensated, δB_z approaches 0 at the compensation point: $B_z = B_c + \delta B_z$. B_e^{eff} is the total effective magnetic field along the z axis experienced by the electron spins: $B_e^{\mathrm{eff}} = B_z + B_n$. When the compensation point is executed, $B_e^{\mathrm{eff}} = \delta B_z - B_e$. Similarly, B_n^{eff} is the total effective field along the z axis experienced by the nuclear spins: $B_n^{\mathrm{eff}} = B_z + B_e = \delta B_z - B_n$.

Equation (5) is the core of our K-Rb-^{21}Ne comagnetometer used for rotation sensing with closed-loop control of the compensation point in this paper. The first dc term is used for rotation sensing, which can be acquired by removing the high-frequency response using the low-pass filter. The dc terms just include the leading rotation dependence terms. When distributing errors of the comagnetometer, a more detailed model has been proposed in our previous research [28]. The second oscillating term is used to realize the closed-loop control of the compensation point by locking electron resonance. The dynamic response takes the form of two overlapping Lorentzian curves centered at $\pm\gamma_e B_e^{\mathrm{eff}}/Q$. Both of the curves have a component with an absorptive lineshape that is in phase with the oscillating field and a component with a dispersive lineshape that is 90° out of phase with the oscillating field. As the electron resonance frequency is much larger than the linewidth under normal K-Rb-^{21}Ne comagnetometer operation, the counter-rotating response centered at $-\gamma_e B_e^{\mathrm{eff}}/Q$ can be ignored [35]. With the compensation point enforced, the amplitude-frequency response $\left|P_x^e(\omega)\right|$ and phase-frequency response $\theta(\omega)$ around the electron resonance can be simplified to the intuitive form

$$\left|P_x^e(\omega)\right| = \frac{\gamma_e B_0 P_z^e}{2\sqrt{(Q\omega + \gamma_e B_e - \gamma_e \delta B_z)^2 + {R_{\mathrm{tot}}^e}^2}}, \quad (7)$$

$$\theta(\omega) = -\arctan\left(\frac{Q\omega + \gamma_e B_e - \gamma_e \delta B_z}{R_{\mathrm{tot}}^e}\right). \quad (8)$$

III. EXPERIMENTAL SETUP AND ELECTRON RESONANCE

The experiment is performed in a dual-axis K-Rb-^{21}Ne comagnetometer, which is used for rotation sensing and is depicted in Fig. 1. A 10-mm-diameter spherical cell made from GE180 aluminosilicate glass, containing a droplet of natural abundance Rb with a small admixture of K, 3 atm ^{21}Ne (70% isotope enriched), and 60 Torr N_2 for quenching, is used. The cell is placed in a boron nitride ceramic oven and heated to 190 °C by a homemade 129-kHz ac electrical heater. At the operating temperature, the Rb vapor density of about 6×10^{14} cm^{-3} is obtained and the density ratio of K to Rb is approximately 1:80. The cell and oven are surrounded by three-layer μ-metal cylindrical magnetic shields and a three-axis magnetic coil system. The magnetic coil system consists of two pairs of saddle coils along the x and y axis, respectively, and two pairs of Lee-Whiting coils with different constants along the z axis. The transverse coils and the larger constant longitudinal coil (Z1 coil) driven by a function generator are used to compensate the residual magnetic fields within the innermost shield, provide transverse field modulation, and set the compensation point. The smaller constant longitudinal coil (Z2 coil) driven by the controller is used to finely control the compensation point. K atoms are optically pumped along the z axis by a 38-mW pump laser, centered on the K D1 resonance line. Rb atoms are polarized by the K atoms through spin-exchange interaction and then they hyperpolarize the ^{21}Ne atoms. The transverse polarization

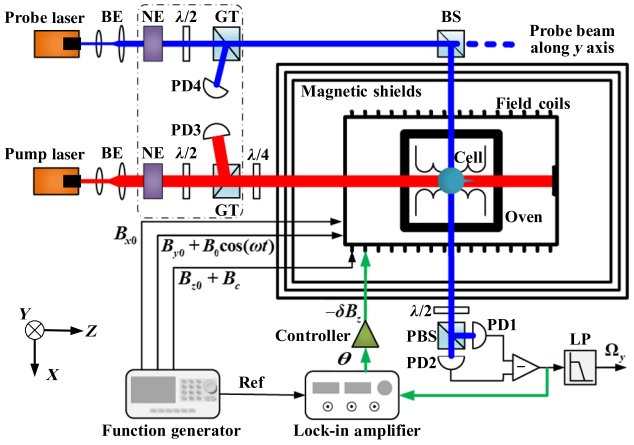

FIG. 1. Schematic of the experimental apparatus. A circularly polarized pump laser propagating along the z axis is used to polarize atoms. A linearly polarized probe laser is split by a beam splitter (BS) to measure the transverse polarization component in the x axis and y axis, respectively, facilitating dual-axis output. The probe beam along the y axis is similar to that along the x axis and the parts into the page are not shown completely. A homemade laser intensity electrocircuit sampling the signal of photodiodes (PD3 and PD4) stabilizes the intensities of the pump laser and probe laser using the noise eaters (NE) as actuators. The output is analyzed by a lock-in amplifier to extract the transverse oscillating field response and then feed back to control the compensation point. The low-pass filter (LP) removes the high-frequency response to extract the rotation sensing signal. The beam expander is denoted as BE; Glan-Taylor polarizer, GT; and polarization beam splitter, PBS.

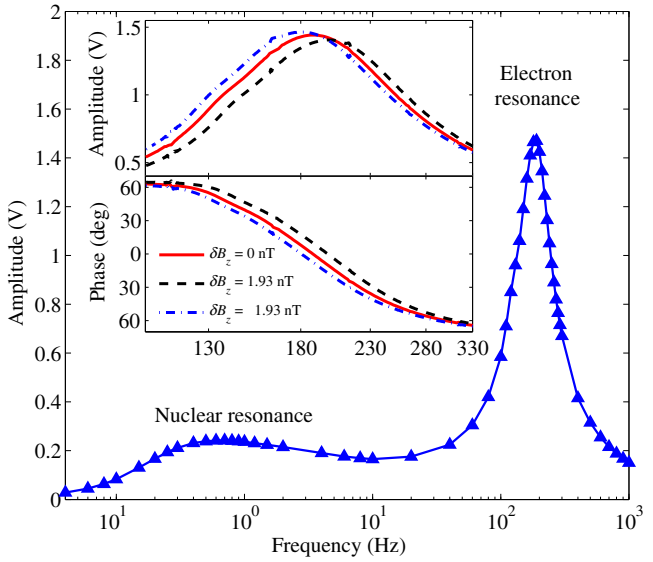

FIG. 2. The frequency response of the K-Rb-^{21}Ne comagnetometer at the compensation point to oscillating fields along the y axis. The electron resonance is clearly separated from the nuclear resonance. The inset shows the amplitude-frequency and phase-frequency response around the electron resonance. The resonance frequency and phase of electrons scale with the shift of the compensation point.

of Rb atoms is measured by optical rotation of a linearly polarized probe laser using about 1 mW and tuned by 0.3 nm to the blue side of the Rb D1 resonance line [36].

Here, we investigate the frequency response of the K-Rb-^{21}Ne comagnetometer to the transverse oscillating magnetic field. A series of magnetic fields with different frequencies and the same peak-to-peak amplitude of 0.15 nT are produced along the y axis. The frequency response measured by the probe beam along the x axis is shown in Fig. 2. The electron resonance separates far away from the nuclear resonance, which is different from that of a K-^{3}He comagnetometer [22]. The discrepancy is owing to the large field from electron magnetization in the Rb-^{21}Ne comagnetometer. When the comagnetometer is operated at the compensation point, the atomic spins experience an effective field opposite to their own magnetic field. That is, the nuclear spins experience an effective field $-B_n$ and the electron spins experience an effective field $-B_e$. The enhancement factor κ_0 in B_e for the Rb-^{21}Ne pair is about 5 times larger than that for the K-^{3}He pair [37,38]. Meanwhile, the density of Rb atoms is about an order higher than that of K atoms in a typical K-^{3}He comagnetometer. Therefore, the electron spins experience a much larger magnetic field in the K-Rb-^{21}Ne comagnetometer, which shifts the electron resonance frequency to a high frequency. The analytic explanation for this phenomenon is presented in Eqs. (5)–(8).

We fit the electron resonance at the compensation point in Fig. 2 by Eq. (7). The electron resonance frequency $\omega_0 = -\gamma_e B_e/Q$ is about 188.0 ± 0.8 Hz and the resonance linewidth $\Delta\omega = R^e_{\rm tot}/Q$ is about 50.1 ± 1.8 Hz. For a typical electron polarization $P^e_z \approx 60\%$ in our experiment, we find $Q \approx 7.5$. Then the electron magnetic field B_e is about -50.4 nT, which is approximately an order of magnitude larger than that in a K-^{3}He comagnetometer. The total electron relaxation rate $R^e_{\rm tot}$ is about 2360.9 s^{-1}, which is highly suppressed from the spin-exchange rate of 5.5×10^5 s^{-1}. Although they experience a large magnetic field in the K-Rb-^{21}Ne comagnetometer, the alkali-metal electron spins are still operated in the SERF regime. The nuclear magnetic field B_n can be derived from subtracting the electron magnetic field B_e from the compensation point B_c, which is about -127.6 nT. The nuclear resonance frequency $\omega_n = -\gamma_n B_n$ is about 0.4 Hz, which is a bit less than the nuclear resonance frequency of about 0.6 Hz in Fig. 2. The discrepancy is ascribed to the coupling of the nuclear spins with the electron spins in the low-frequency domain. The nuclear resonance frequency approximately represents the bandwidth of the comagnetometer for rotation sensing. Deviating from the compensation point could decrease the bandwidth of the SERF comagnetometer [22]. Therefore, closed-loop control of the compensation point could stabilize the bandwidth at the optimal value.

IV. RESULT AND DISCUSSION

From the amplitude-frequency response in Eq. (7) and phase-frequency response in Eq. (8), we can see that the electron resonance frequency and phase scale with the shift of the compensation point δB_z and the result measured by the probe beam along the x axis is shown in the inset of Fig. 2. This phenomenon inspires the closed-loop control of the compensation point by locking the electron resonance. To accomplish this, a feedback control system is incorporated in our apparatus, which is depicted in Fig. 1. A field modulated at the electron resonance frequency ω_0 is applied along the y axis; the signal is read out by the probe beam along the x axis and demodulated by the lock-in amplifier with $\cos(\omega_0 t)$. The demodulated phase $\theta = \arctan\left(\gamma_e \delta B_z / R^e_{\rm tot}\right)$ is fed through the controller. The controller compares the demodulated phase with the initial electron resonance phase and then powers the Z2 coil to keep the electron resonance constant. The performance of the closed-loop control system is presented hereafter.

Firstly, we evaluate the performance of the closed-loop control method by changing the δB_z field around the compensation point. We slowly scan the δB_z field from -10 to 10 nT using the Z1 coil under the open-loop scheme and closed-loop scheme. The scanning magnetic field, demodulated phase at the driving frequency, and signal of the comagnetometer are synchronously recorded by a National Instrument 24-bit data acquisition system with the sampling rate of 200 Hz. The original data are shown in Fig. 3. The residual magnetic fields B_x and B_y, rotations Ω_x and Ω_y, and light shift fields L_x and L_z cannot be zeroed completely, which introduces a δB_z dependence to the comagnetometer signal [28],

$$P^e_x(\delta B_z) \approx \frac{-\gamma_e^2 P^e_z \delta B_z}{{R^e_{\rm tot}}^2 B_n}\left[\left(B_x + \frac{Q\Omega_x}{\gamma_e} + L_x\right)\delta B_z + L_z B_x + \frac{R^e_{\rm tot} B_y}{\gamma_e} - \frac{B_c \Omega_x}{\gamma_n} + \frac{Q R^e_{\rm tot}\Omega_y}{\gamma_e^2} + B_c L_x\right]. \quad (9)$$

When the comagnetometer is operated in the open-loop scheme, which is shown in Fig. 3(a), the demodulated phase at driving frequency ω_0 response to δB_z scanning is consistent with the theoretical expression $\theta = \arctan\left(\gamma_e \delta B_z / R^e_{\rm tot}\right)$, while the signal of the comagnetometer drifts with δB_z scanning and the profile is a quadratic function corresponding to Eq. (9). When the comagnetometer is operated in the closed-loop scheme, which is shown in Fig. 3(b), by locking the electron resonance, δB_z is real-time compensated by feedback electronics automatically; thus the demodulated phase and the signal of the comagnetometer remain constant. The results verify the feasibility of the method we proposed. With the closed-loop control of the compensation point, the comagnetometer is unaffected by the fluctuation of the longitudinal residual magnetic field.

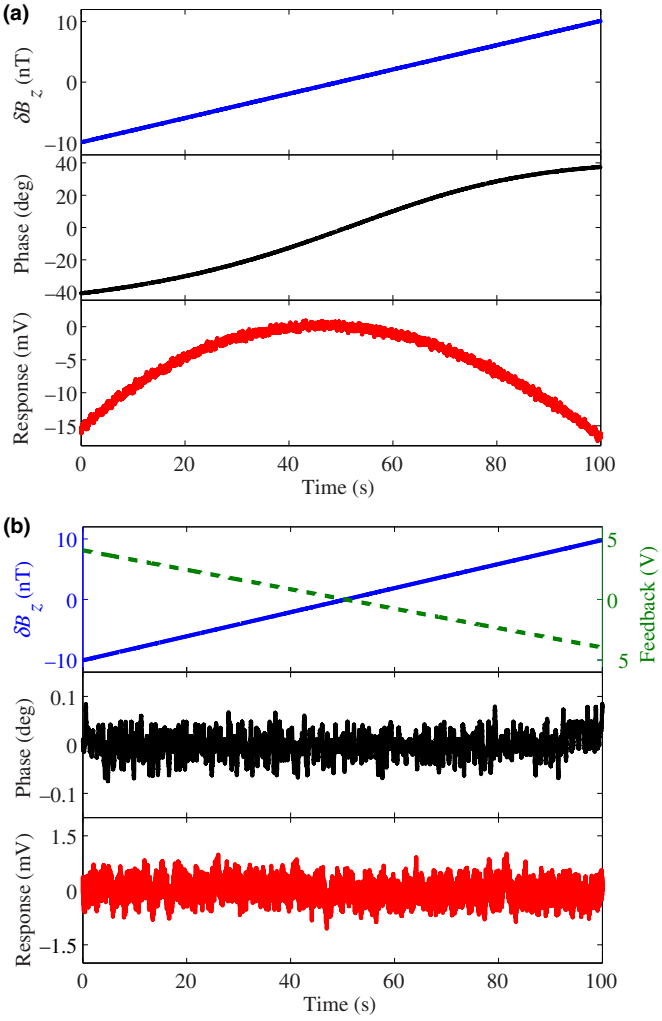

FIG. 3. Demodulated phase at driving frequency ω_0 and signal of the comagnetometer response to the shift of the compensation point scanning from -10 to 10 nT in (a) the open-loop scheme and (b) the closed-loop scheme. The δB_z field can be real-time canceled by the feedback electronics under the closed-loop scheme. The signal offset at the compensation point is set to zero. By stabilizing the demodulated phase at electron resonance, the comagnetometer is free from the drift of the longitudinal magnetic field in the closed-loop scheme.

Secondly, we evaluate the transient response of the closed-loop system following a sudden step in the δB_z field. The result is shown in Fig. 4. When the comagnetometer is operated in the closed-loop scheme and a 5-nT step magnetic field is applied along the z axis by the Z1 coil, the PID controller quickly outputs a feedback signal to drive the Z2 coil and cancel the step magnetic field, bringing the demodulated phase at driving frequency and the signal of the comagnetometer back to the steady state. The transient time is about 0.7 s, which is restricted by the control algorithm and slow precession of the noble-gas nuclear spins. The closed-loop control method presented here is effective and robust against the sudden disturbance.

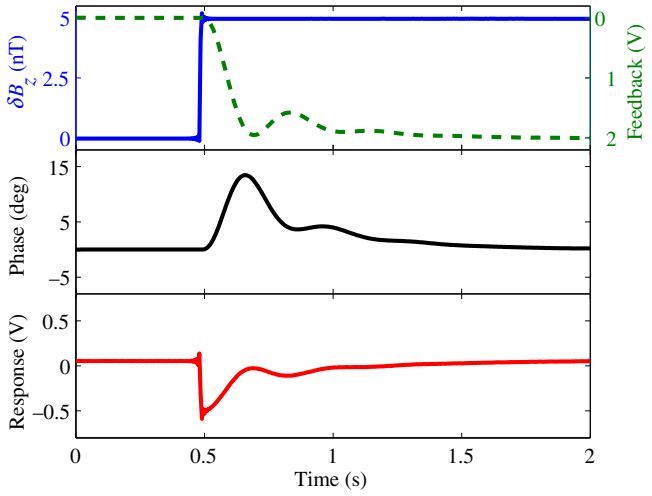

FIG. 4. The transient response of the closed-loop control system to the sudden step of the shift of the compensation point δB_z. The feedback electronics quickly cancel the step magnetic field and bring the demodulated phase at driving frequency and the signal of the comagnetometer back to the steady state. The closed-loop control method is robust against the sudden disturbance.

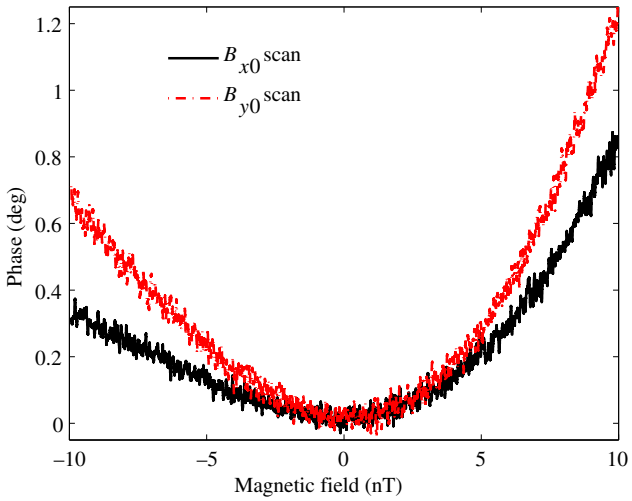

FIG. 5. The demodulated phase at the driving frequency response to the scans of magnetic field B_{x0} along the x axis and B_{y0} along the y axis. They both approach the minimum at the zero field and increase when nuclear spin polarization $\mathbf{P^n}$ precesses away from the z axis to compensate the transverse residual magnetic field.

Thirdly, we consider the effect of fluctuation of the nuclear magnetization. δB_z is constantly drifting on account of drifting nuclear spin polarization. Moreover, when the transverse excitations are large, $\mathbf{P^n}$ precesses a large angle away from the z axis and the assumption that P_z^n is constant in Sec. II is not valid. We begin with implementing large transverse magnetic-field excitations on the comagnetometer under the open-loop scheme. Similarly, we slowly scan the fields B_{x0} along the x axis and B_{y0} along the y axis from -10 to 10 nT, respectively. The demodulated phase at the driving frequency is recorded by the data acquisition system and shown in Fig. 5. The change of the demodulated phase following the B_{x0} scan is analogous to that following the B_{y0} scan and they both approach the minimum at the zero field. We ascribe this result to the precession of the nuclear spin polarization $\mathbf{P^n}$. When operated at the compensation point, nuclear spin polarization $\mathbf{P^n}$ adiabatically follows slow changes in the external magnetic field, decreasing the effect of transverse fields on alkali-metal electrons. With the angle between the nuclear spin polarization $\mathbf{P^n}$ and the z axis increasing, the compensation magnetic field B_c is gradually greater than the actual compensation point under the open-loop scheme, $\delta B_z > 0$, which increases the demodulated phase according to Eq. (8) and Fig. 3(a).

For further explanation, we use a rotating platform with an accuracy of 0.001 deg/s to provide the transverse excitations. The y axis of the comagnetometer is mounted vertically and aligned with the rotating axis of the platform. According to Eqs. (5) and (6), when inputting Ω_y, the signal measured by the probe beam along the x axis is defined as the sensitive response and shown in Eq. (10). Meanwhile, the signal measured by the probe beam along the y axis arising from the detuning of the compensation point δB_z is defined as the coupling response and shown in Eq. (11):

$$P_x^e(\Omega_y) = \frac{-\gamma_e P_z^e R_{\rm tot}^e \Omega_y/\gamma_n}{{R_{\rm tot}^e}^2+\gamma_e^2\left[{\delta B_z}^2+\left(\Omega_y/\gamma_n\right)^2\right]}, \tag{10}$$

$$P_y^e(\Omega_y) = \frac{-\gamma_e^2 P_z^e \delta B_z \Omega_y/\gamma_n}{{R_{\rm tot}^e}^2+\gamma_e^2\left[{\delta B_z}^2+\left(\Omega_y/\gamma_n\right)^2\right]}. \tag{11}$$

The experimental result is shown in Fig. 6. When the comagnetometer is operated in the open-loop scheme, the equilibrium angle between $\mathbf{P^n}$ and the z axis increases with the input rotation rate increasing. The stationary bias field B_c gradually deviates from the actual compensation point and causes a nonzero δB_z field. The nonzero δB_z decreases the response of the sensitive axis and creates a severe cross-talk response in the coupling axis, which is consistent with Eqs. (10) and (11). When the comagnetometer is operated in the closed-loop scheme, the nonzero δB_z is real-time canceled by the feedback electronics, leaving the compensation point tuned all the time. This improves the scale factor linearity, enlarges the measuring range, and suppresses the cross-talk error of the comagnetometer. The minor fluctuation of the coupling response around zero in the closed-loop scheme can be further removed by optimizing the control algorithm and parameters.

The limited measuring range in the closed-loop scheme is restricted by the characteristics of the atom spins, which

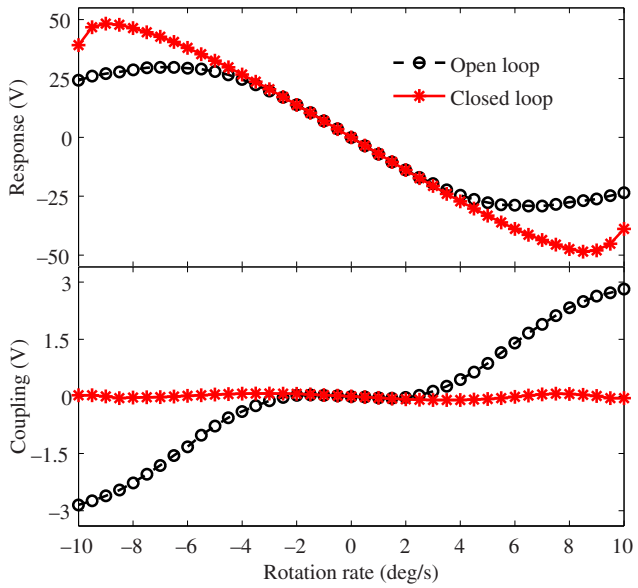

FIG. 6. The dual-axis comagnetometer response to rotation rate inputting along the y axis operated in the open-loop scheme and closed-loop scheme. Top: The sensitive response P_x^e measured by the probe beam along the x axis. Bottom: The coupling response P_y^e measured by the probe beam along the y axis. The closed-loop control of the compensation point could extend the linear measurement range and suppress the cross-talk error of the comagnetometer.

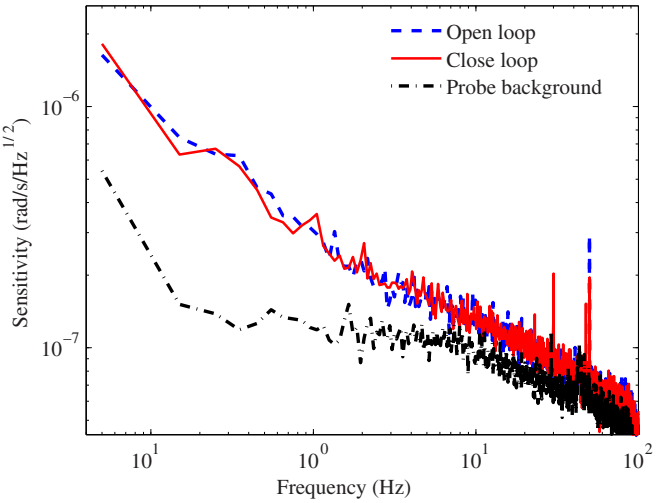

FIG. 7. The rotation sensitivities of the comagnetometer operated in the open-loop scheme and closed-loop scheme. The probe background noise obtained in the absence of the pump laser is also shown. The sensitivities of both schemes are the same and not limited by the probe background noise.

are given by $\Omega_{\max} = \pm\gamma_n R^e_{\rm tot}/\gamma_e$. While the rotation uncertainty per unit bandwidth is given by $\delta\Omega = (\gamma_n/\gamma_e) \times \left[R^e_{\rm tot} Q/(nV)\right]^{1/2}$, where n is the density of alkali-metal atoms and V is the measurement volume [9]. In the future, we should solve the contradiction between the high sensitivity and large measuring range of the SERF comagnetometer; furthermore, a closed-loop detection method, which could stabilize the nuclear and electron spins at the equilibrium state, is required to extend the measuring range and bandwidth.

Finally, the rotation sensitivities of the comagnetometer operated in the open-loop scheme and closed-loop scheme are measured and compared in Fig. 7. The probe background noise is also obtained in the absence of the pump laser. The output signals are acquired by the data acquisition system with the sampling rate of 200 Hz. The scale factor obtained from Fig. 6 is used for converting the output voltage signal to the rotation rate signal. Then the power spectral density is calculated and averaged for each 0.1-Hz bin. The rotation sensitivities of both the open-loop scheme and closed-loop scheme are almost the same and not limited by the probe background noise. In the K-Rb-^{21}Ne comagnetometer we build, though the compensation point is controlled, which is the longitudinal magnetic field, the transverse magnetic noise coming from the innermost magnetic shield still dominates the rotation sensitivity and prevents the improvement of low-frequency sensitivity in the closed-loop scheme.

V. CONCLUSION

In conclusion, we investigate the transverse oscillating field response of the K-Rb-^{21}Ne comagnetometer and found that the electron resonance is shifted to a high frequency and separated far away from the nuclear resonance owing to the large field from electron magnetization, which is different from that of a K-^{3}He comagnetometer. By locking the separated electron resonance, we demonstrate a real-time closed-loop control method to stabilize the compensation point of the K-Rb-^{21}Ne comagnetometer, both theoretically and experimentally. The technique presented here could improve the systematic stability, enlarge the linear measuring range, and suppress the cross-talk error of the comagnetometer. Our work will be important for precision metrology applications using the SERF comagnetometer [39] and sheds light on the way to introduce an atom-related closed-loop control technique into the SERF comagnetometer.

ACKNOWLEDGMENTS

We would like to thank Wenfeng Wu and Yan Yin for useful discussions. This work was supported by the National Key R&D Program of China under Grants No. 2016YFB0501600 and No. 2016YFA0301500; the NSFC under Grants No. 61773043, No. 61473268, No. 61503353, No. 11434015, and No. 61835013; SPRPCAS under Grants No. XDB01020300 and No. XDB21030300;

and the Academic Excellence Foundation of BUAA for PhD Students.

[1] D. Bear, R. E. Stoner, R. L. Walsworth, V. A. Kostelecký, and C. D. Lane, Limit on Lorentz and CPT Violation of the Neutron Using a Two-species Noble-gas Maser, Phys. Rev. Lett. **85**, 5038 (2000).

[2] V. A. Kostelecký and N. Russell, Data tables for Lorentz and CPT violation, Rev. Mod. Phys. **83**, 11 (2011).

[3] M. Smiciklas, J. M. Brown, L. W. Cheuk, S. J. Smullin, and M. V. Romalis, New Test of Local Lorentz Invariance Using a ^{21}Ne-Rb-K Comagnetometer, Phys. Rev. Lett. **107**, 171604 (2011).

[4] F. Allmendinger, W. Heil, S. Karpuk, W. Kilian, A. Scharth, U. Schmidt, A. Schnabel, Y. Sobolev, and K. Tullney, New Limit on Lorentz-invariance- and CPT-violating Neutron Spin Interactions Using a Free-spin-precession ^{3}He-^{129}Xe Comagnetometer, Phys. Rev. Lett. **112**, 110801 (2014).

[5] G. Vasilakis, J. Brown, T. Kornack, and M. Romalis, Limits on New Long Range Nuclear Spin-dependent Forces Set with a K-^{3}He Comagnetometer, Phys. Rev. Lett. **103**, 261801 (2009).

[6] M. Bulatowicz, R. Griffith, M. Larsen, J. Mirijanian, C. Fu, E. Smith, W. Snow, H. Yan, and T. Walker, Laboratory Search for a Long-range T-odd, P-odd Interaction from Axionlike Particles Using Dual-species Nuclear Magnetic Resonance with Polarized ^{129}Xe and ^{131}Xe gas, Phys. Rev. Lett. **111**, 102001 (2013).

[7] L. Hunter, J. Gordon, S. Peck, D. Ang, and J.-F. Lin, Using the earth as a polarized electron source to search for long-range spin-spin interactions, Science **339**, 928 (2013).

[8] D. F. Jackson Kimball, J. Dudley, Y. Li, D. Patel, and J. Valdez, Constraints on long-range spin-gravity and monopole-dipole couplings of the proton, Phys. Rev. D **96**, 075004 (2017).

[9] T. Kornack, R. Ghosh, and M. Romalis, Nuclear Spin Gyroscope Based on an Atomic Comagnetometer, Phys. Rev. Lett. **95**, 230801 (2005).

[10] E. A. Donley, in *2010 IEEE Sensors* (IEEE, 2010), p. 17.

[11] M. E. Limes, D. Sheng, and M. V. Romalis, ^{3}He-^{129}Xe Comagnetometery Using ^{87}Rb Detection and Decoupling, Phys. Rev. Lett. **120**, 033401 (2018).

[12] L. Jiang, W. Quan, R. Li, W. Fan, F. Liu, J. Qin, S. Wan, and J. Fang, A parametrically modulated dual-axis atomic spin gyroscope, Appl. Phys. Lett. **112**, 054103 (2018).

[13] C. Zhang, H. Yuan, Z. Tang, W. Quan, and J. Fang, Inertial rotation measurement with atomic spins: From angular momentum conservation to quantum phase theory, Appl. Phys. Rev. **3**, 041305 (2016).

[14] C. A. Baker, D. D. Doyle, P. Geltenbort, K. Green, M. G. D. van der Grinten, P. G. Harris, P. Iaydjiev, S. N. Ivanov, D. J. R. May, J. M. Pendlebury, J. D. Richardson, D. Shiers, and K. F. Smith, Improved Experimental Limit on the Electric Dipole Moment of the Neutron, Phys. Rev. Lett. **97**, 131801 (2006).

[15] D. Sheng, A. Kabcenell, and M. V. Romalis, New Classes of Systematic Effects in Gas Spin Comagnetometers, Phys. Rev. Lett. **113**, 163002 (2014).

[16] S. K. Lamoreaux, J. P. Jacobs, B. R. Heckel, F. J. Raab, and E. N. Fortson, New Limits on Spatial Anisotropy from Optically-pumped ^{201}Hg and ^{199}Hg, Phys. Rev. Lett. **57**, 3125 (1986).

[17] E. Kanegsberg, Nuclear magnetic resonance gyroscope, U.S. Patent No. 7,282,910 (2007).

[18] F. Allmendinger, U. Schmidt, W. Heil, S. Karpuk, Y. Sobolev, and K. Tullney, in *International Journal of Modern Physics: Conference Series* (World Scientific, 2016), Vol. 40, p. 1660082.

[19] B. C. Grover, E. Kanegsberg, J. G. Mark, and R. L. Meyer, Nuclear magnetic resonance gyro, U.S. Patent No. 4,157,495 (1979).

[20] D. Meyer and M. Larsen, Nuclear magnetic resonance gyro for inertial navigation, Gyroscopy Navig. **5**, 75 (2014).

[21] T. Walker and M. Larsen, Spin-exchange-pumped NMR gyros, Adv. At. Mol. Opt. Phys. **65**, 373 (2016).

[22] T. Kornack and M. Romalis, Dynamics of Two Overlapping Spin Ensembles Interacting by Spin Exchange, Phys. Rev. Lett. **89**, 253002 (2002).

[23] J. M. Brown, S. J. Smullin, T. W. Kornack, and M. V. Romalis, New Limit on Lorentz- and CPT-violating Neutron Spin Interactions, Phys. Rev. Lett. **105**, 151604 (2010).

[24] J. Fang, Y. Chen, Y. Lu, W. Quan, and S. Zou, Dynamics of Rb and ^{21}Ne spin ensembles interacting by spin exchange with a high Rb magnetic field, J. Phys. B **49**, 135002 (2016).

[25] W. Happer and A. C. Tam, Effect of rapid spin exchange on the magnetic-resonance spectrum of alkali vapors, Phys. Rev. A **16**, 1877 (1977).

[26] J. C. Allred, R. N. Lyman, T. W. Kornack, and M. V. Romalis, High-sensitivity Atomic Magnetometer Unaffected by Spin-exchange Relaxation, Phys. Rev. Lett. **89**, 130801 (2002).

[27] R. Li, W. Quan, W. Fan, L. Xing, and J. Fang, Influence of magnetic fields on the bias stability of atomic gyroscope operated in spin-exchange relaxation-free regime, Sens. Actuator A-Phys. **266**, 130 (2017).

[28] L. Jiang, W. Quan, R. Li, L. Duan, W. Fan, Z. Wang, F. Liu, L. Xing, and J. Fang, Suppression of the cross-talk effect in a dual-axis K-Rb-^{21}Ne comagnetometer, Phys. Rev. A **95**, 062103 (2017).

[29] Y. Chen, W. Quan, L. Duan, Y. Lu, L. Jiang, and J. Fang, Spin-exchange collision mixing of the K and Rb ac Stark shifts, Phys. Rev. A **94**, 052705 (2016).

[30] W. Happer, G. D. Cates Jr, M. V. Romalis, and C. J. Erickson, Alkali metal hybrid spin-exchange optical pumping, U.S. Patent No. 6,318,092 (2001).

[31] E. Babcock, I. Nelson, S. Kadlecek, B. Driehuys, L. W. Anderson, F. W. Hersman, and T. G. Walker, Hybrid Spin-exchange Optical Pumping of ^{3}He, Phys. Rev. Lett. **91**, 123003 (2003).

[32] S. Appelt, A. B.-A. Baranga, C. J. Erickson, M. V. Romalis, A. R. Young, and W. Happer, Theory of spin-exchange optical pumping of ^{3}He and ^{129}Xe, Phys. Rev. A **58**, 1412 (1998).

[33] S. R. Schaefer, G. D. Cates, T.-R. Chien, D. Gonatas, W. Happer, and T. G. Walker, Frequency shifts of the magnetic-resonance spectrum of mixtures of nuclear spin-polarized noble gases and vapors of spin-polarized alkali-metal atoms, Phys. Rev. A **39**, 5613 (1989).

[34] R. Li, W. Fan, L. Jiang, L. Duan, W. Quan, and J. Fang, Rotation sensing using a K-Rb-^{21}Ne comagnetometer, Phys. Rev. A **94**, 032109 (2016).

[35] J. Lu, Z. Qian, and J. Fang, A fast determination method for transverse relaxation of spin-exchange-relaxation-free magnetometer, Rev. Sci. Instrum. **86**, 043104 (2015).

[36] D. Budker, W. Gawlik, D. F. Kimball, S. M. Rochester, V. V. Yashchuk, and A. Weis, Resonant nonlinear magneto-optical effects in atoms, Rev. Mod. Phys. **74**, 1153 (2002).

[37] R. Stoner and R. Walsworth, Measurement of the ^{21}Ne zeeman frequency shift due to Rb-^{21}Ne collisions, Phys. Rev. A **66**, 032704 (2002).

[38] E. Babcock, I. A. Nelson, S. Kadlecek, and T. G. Walker, ^{3}He polarization-dependent EPR frequency shifts of alkali-metal-^{3}He pairs, Phys. Rev. A **71**, 013414 (2005).

[39] V. V. Flambaum and M. V. Romalis, Limits on Lorentz Invariance Violation from Coulomb Interactions in Nuclei and Atoms, Phys. Rev. Lett. **118**, 142501 (2017).